Journal of Hydrology: Regional Studies 58 (2025) 102270

Contents lists available at ScienceDirect

Journal of Hydrology: Regional Studies

journal homepage: www.elsevier.com/locate/ejrh

Compound temporal-spatial extreme precipitation events in the Poyang Lake Basin of China

Chao Deng [a,b], Yinchi Zhang [a,b], Miaomiao Ma [c], Ying Chen [a,b,d,e], Jianhui Wei [f], Harald Kunstmann [f], Lu Gao [a,b,d,e,*]

[a] Key Laboratory for Humid Subtropical Eco-geographical Processes of the Ministry of Education, Fujian Normal University, Fuzhou 350117, China
[b] Institute of Geography, Fujian Normal University, Fuzhou 350117, China
[c] China Institute of Water Resources and Hydropower Research, Beijing 100038, China
[d] School of Geographical Sciences, Fujian Normal University, Fuzhou 350117, China
[e] Fujian Provincial Engineering Research Center for Monitoring and Accessing Terrestrial Disasters, Fujian Normal University, Fuzhou 350117, China
[f] Institute of Meteorology and Climate Research (IMKIFU), Karlsruhe Institute of Technology, Campus Alpin, Garmisch-Partenkirchen, Germany

ARTICLE INFO

Keywords:
Persistent extreme precipitation
Widespread extreme precipitation
Compound events
WRF
Poyang Lake Basin

ABSTRACT

Study region: The study region is the Poyang Lake Basin (PLB). As a typical humid subtropical basin in China, the PLB is crisscrossed by rivers and lakes, where frequent hydrological and meteorological processes occur.

Study focus: This study identified temporal extreme precipitation, spatial extreme precipitation, and compound temporal-spatial extreme precipitation events to investigate precipitation extremes. The differences in occurrence of compound widespread-persistent extreme precipitation (WPEP), persistent extreme precipitation (PEP) and widespread extreme precipitation (WEP) events were investigated using the Weather Research and Forecast (WRF) model.

New hydrological insights for the region: Extreme precipitation events characterized by high intensity and long duration were more likely to occur in the northern part of the PLB. The frequency of extreme precipitation showed an increasing trend in the central and northeastern regions of the PLB. The contribution of PEP increased from an average of 30.7 % during the period 1983–1992 to 37.2 % during 2013–2022. The WPEP event exhibited a prolonged duration, greater precipitation intensity, and higher precipitable water (PW) and water vapor mixing ratio at 2 m (Q2). Significant changes in PW and Q2 were observed prior to the occurrence of the PEP event. However, PW and Q2 values remained stable during WEP and WPEP events. The PLB was influenced by two water vapor sources, from the north and southwest during the WEP and WPEP events.

1. Introduction

Under the global warming, changes in atmospheric conditions and acceleration of the water cycle tend to trigger more extreme weather events, such as heavy rains, droughts, and heatwaves (Donat et al., 2016; Myhre et al., 2019; Shibuya et al., 2021; Kang et al., 2022; Tan et al., 2023). Precipitation is a primary driver of the terrestrial water cycle. The contribution of global precipitation to land

* Corresponding author at: Key Laboratory for Humid Subtropical Eco-geographical Processes of the Ministry of Education, Fujian Normal University, Fuzhou 350117, China.
E-mail address: l.gao@foxmail.com (L. Gao).

https://doi.org/10.1016/j.ejrh.2025.102270
Received 2 January 2025; Received in revised form 17 February 2025; Accepted 21 February 2025
Available online 28 February 2025

water storage exceeds 64 % (Zhong et al., 2025). Recent research has demonstrated a significant upward trend in the frequency and intensity of extreme precipitation events across global regions (Janssen et al., 2016; Papalexiou and Montanari, 2019; Thackeray et al., 2022; Tuel et al., 2022). China also experiences a significant increase in extreme precipitation, especially heavy rainfall triggered by tropical cyclones along the southeast coast, as well as convective rainstorms in southern China and the Yangtze River basin (Sun and Ao, 2013; Zhu et al., 2021; Yang et al., 2022; Wu et al., 2023). Extreme precipitation has become a critical environmental hazard, not only causing urban flooding but also triggering severe natural disasters such as flash floods, landslides, and mudslides. The occurrence of extreme precipitation events poses a major threat to agricultural production, socio-economis and ecosystems (Lesk et al., 2016; Gründemann et al., 2023; Ombadi et al., 2023). In recent years, widespread flooding caused by extreme precipitation has been observed globally. For example, floods associated with extreme rainfall cause annual losses of approximately $3 billion in India (Roxy et al., 2017; Pal et al., 2021). Similarly, the rainstorm that struck western Europe in 2021 triggered a large-scale flood, resulting in a loss of 46 billion euros and a large number of casualties (Tuel et al., 2022). In the summer of 2016, south China experienced deadly floods, which affected around 32 million people across 26 provinces (Tang et al., 2017). These phenomena indicate that extreme precipitation significantly increase the risk of flooding (Roxy et al., 2017; Zhang et al., 2017; Rastogi et al., 2020).

An understanding of variations of extreme precipitation is of great significance for reducing the risk of hydrological disasters under global warming(Yin et al., 2018; Xie et al., 2023). Accurate precipitation information is essential for exploring the characteristics and mechanisms of extreme precipitation. Global Glimate Models (GCMs) have become critical tools for analyzing climate change and extreme precipitation events through large-scale climate simulations (Smalley et al., 2019). However, it is often difficult for GCMs to accurately represent localized rainfall patterns due to the relatively coarse resolution, which makes it challenging to simulate the complex dynamics of small-scale extreme events such as convective heavy rainfall (Jiang et al., 2021). This limitation is addressed by high-resolution regional climate models that perform well in capturing the interaction processes between weather systems and the land surface (Glisan et al., 2013; Yang et al., 2021). Among them, the Weather Research and Forecast model (WRF), as a new generation of mesoscale high-resolution prediction models, is capable of describing land-atmosphere continuum processes in a specific region with complicated topography (Ojeda et al., 2017; Tian et al., 2020; Deng et al., 2023). The ability of WRF to simulate atmospheric anomalies in a variety of complex scenarios provides new ways to capture extreme precipitation processes and understand the drivers and physical mechanisms of extreme precipitation events.

The contribution of extreme precipitation is influenced by multiple factors. Extreme precipitation events are generally attributed to the large-scale circulation drivers such as the sea surface temperature, intraseasonal oscillations (Pei et al., 2018; Ning et al., 2021). Moreover, the formation and development of precipitation may be complicated by various regional surface attributes, including mesoscale topography and large urban agglomerations (Zhu et al., 2021). As rainstorms characterized by widespread, prolonged and damaging occur frequently, precipitation extremes are becoming more prominent. When precipitation covers a sufficiently large area, it can trigger larger scale floods and urban waterlogging (Cassano et al., 2016; Moore et al., 2019). The impact of extreme precipitation with a long duration on the region is greater than that of an ordinary rainstorm (Wan et al., 2017; Du et al., 2019; Cheng et al., 2023). Especially the co-occurrence of persistent extreme precipitation and widespread extreme precipitation brings more severe socio-economic losses and environmental impacts than individual events (Gründemann et al., 2023).

Previous studies tend to ignore regional characteristics of duration and coverage in extreme precipitation processes (Cassano et al., 2016; Papalexiou and Montanari, 2019; Cheng et al., 2023). In particular, few studies pay attention to the compound events of persistent extreme precipitation and widespread extreme precipitation. The Poyang Lake Basin (PLB) is as a representative area for extreme precipitation study (Dong et al., 2011; Li and Hu, 2019). This study aimed to investigate the differences in the occurrence of persistent extreme precipitation (PEP), widespread extreme precipitation (WEP), and widespread-persistent compound extreme precipitation (WPEP) using WRF simulations. Additionally, the surface processes and meteorological conditions associated with PEP, WEP, and WPEP events in the PLB were analyzed. The findings are expected to contribute to more effective flood prevention and disaster risk mitigation in the context of climate change.

2. Data and Method

2.1. Definition of extreme precipitation

Extreme precipitation events are described as occurrences where precipitation exceeds a predetermined threshold. The 95th percentile of daily precipitation from 1983 to 2022 is chosen as the threshold for extreme precipitation at each individual grid point. Thus, any daily precipitation exceeding this threshold is classified as an extreme precipitation event, excluding days without precipitation (less than 0.1 mm). The simple index of extreme precipitation frequency (SEPF) and the simple index of extreme daily precipitation intensity (SDPI) are used as indicators to quantify the frequency and intensity of extreme precipitation events, respectively (Pei et al., 2018). The calculation of two indices is outlined as follows:

$$\mathrm{SEPF} = \sum_{j=1}^{365} \mathrm{T}_{yd} \tag{1}$$

where T_{yd} is a conditional function. When P_d (daily precipitation on day d) exceeds the extreme precipitation threshold during the year y, then T_{yd} is equal to 1. Otherwise, T_{yd} is equal to 0, which means that no extreme precipitation events occurs during this period.

$$SDPI = \frac{\left(\sum_{d=1}^{365} P_{yd}\right)}{N_y} \quad (2)$$

where P_{yd} (P_{yd}> extreme precipitation threshold) is the daily precipitation on day d of year y, and N_y is the number of extreme precipitation events occurring in year y.

Based on the duration of extreme precipitation, precipitation events are categorized into non-persistent and persistent extreme precipitation (Wan et al., 2017). A persistent extreme precipitation (PEP) event is characterized by daily precipitation exceeding the extreme precipitation threshold for at least two consecutive days, and the first day of extreme precipitation is considered as the beginning of a persistent extreme precipitation event (He and Zhai, 2018). Furthermore, it defines a widespread extreme precipitation (WEP) event as simultaneous occurrence of extreme precipitation over at least N grid points in study region (Cassano et al., 2016; Shibuya et al., 2021). In this context, widespread extreme precipitation events are classified into two types based on grid point counts exceeding 50 % and 70 %, respectively. The simultaneous occurrence of widespread extreme precipitation and persistent extreme precipitation events is regarded as a compound widespread-persistent extreme precipitation (WPEP) event. Specifically, such compound events are identified when daily extreme precipitation covers at least 50 % of the grid points within the study area and persists at least two consecutive days.

2.2. Study area

The Poyang Lake Basin (PLB), which located in the middle and lower reaches of the Yangtze River Basin, exhibits a distinctive pattern of alternating dry and wet conditions (Lei et al., 2021; Deng et al., 2024). The Poyang Lake within the basin is the largest freshwater lake in China and also an important flood storage lake in the Yangtze River Basin. The PLB has five sub-basins, including Xiushui (sub-basin size: 3548 km^2), Ganjiang (80948 km^2), Fuhe (15811 km^2), Xinjiang (15535 km^2), and Raohe (6374 km^2) (Fig. 1). The spatial distribution of precipitation within this basin displays significant unevenness, characterized by distinct seasonal patterns. Precipitation is concentrated during the months of April to June, which consequently results in recurrent summer flooding (Zhang et al., 2015).

2.3. Datasets

Daily precipitation data utilized in this study are sourced from a new daily gridded precipitation dataset based on gauge observations for the Chinese mainland. This dataset is provided by the National Tibetan Plateau/ Third Pole Environment Data Center (Gou et al., 2021; Miao et al., 2022; Han et al., 2023). The spatial resolution of dataset is 0.1° x 0.1°. The Final Operational Global Analysis (FNL) reanalysis data from the National Centers for Environmental Prediction are used for initial and boundary fields of the WRF simulation, with a horizontal resolution of 1° x 1°, a temporal resolution of 6 h, and 26 vertical pressure levels. The topographic data used for the WRF simulations are obtained from the USGS provided by the United States Geological Survey.

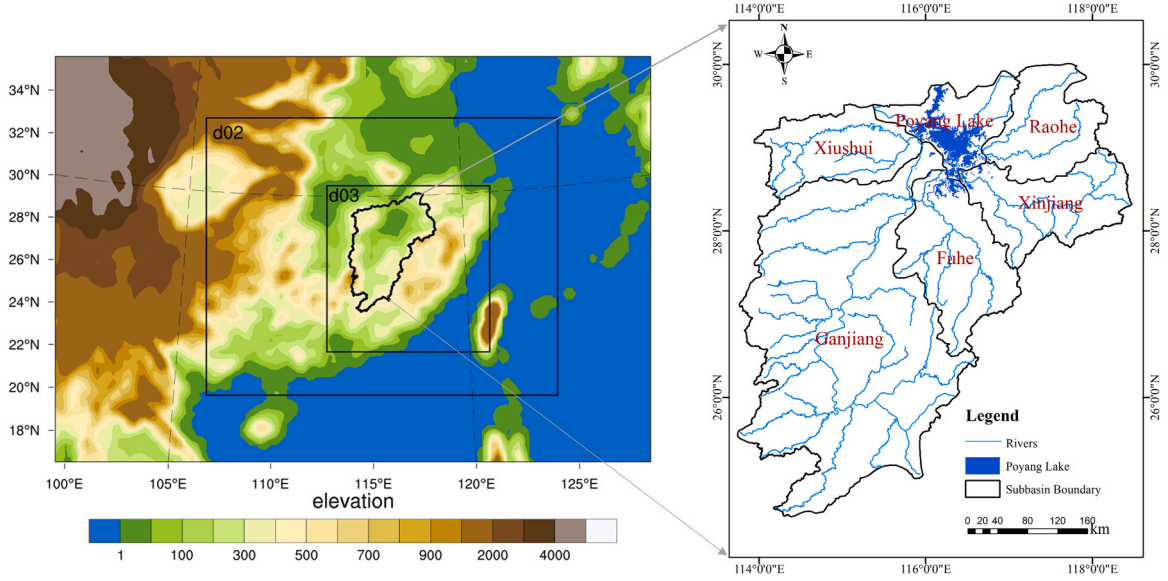

Fig. 1. The three WRF domains and stream networks in the Poyang Lake Basin.

2.4. WRF model setup

WRF version 4.3 is selected to simulate extreme precipitation events. The WRF simulation is configured with three nested domains, featuring horizontal resolutions of 27 km (d01), 9 km (d02), and 3 km (d03) (Fig. 1). The horizontal coordinates of the model are projected using the Lambert conformal conic projection. The time steps in the WRF simulation are set at 90 seconds. Simulation output is generated every six hours. The domain sizes are configured as 115 × 79, 202 × 160, and 280 × 286, respectively. The simulated extreme precipitation events include the PEP event (June 2–11, 2019), the WPEP event (July 3–12, 2020), and the WEP event (June 24–July 3, 2021). The initial 36 hours of each simulation are designated as the model start-up time and their results are excluded from analysis. The selection of the physical parameterization scheme for the WRF is based on previous sensitivity studies in the PLB (Deng et al., 2023; Wu et al., 2023). The chosen combination of physical parameterization schemes in the model includes the New Tiedtke (NT) scheme, Thompson scheme, Noah scheme, Rapid Radiative Transfer Model (RRTM) long wave radiation scheme, Dudhia short wave radiation scheme and Yonsei University (YSU) planetary boundary layer scheme. In addition, it should be noted that the cumulus

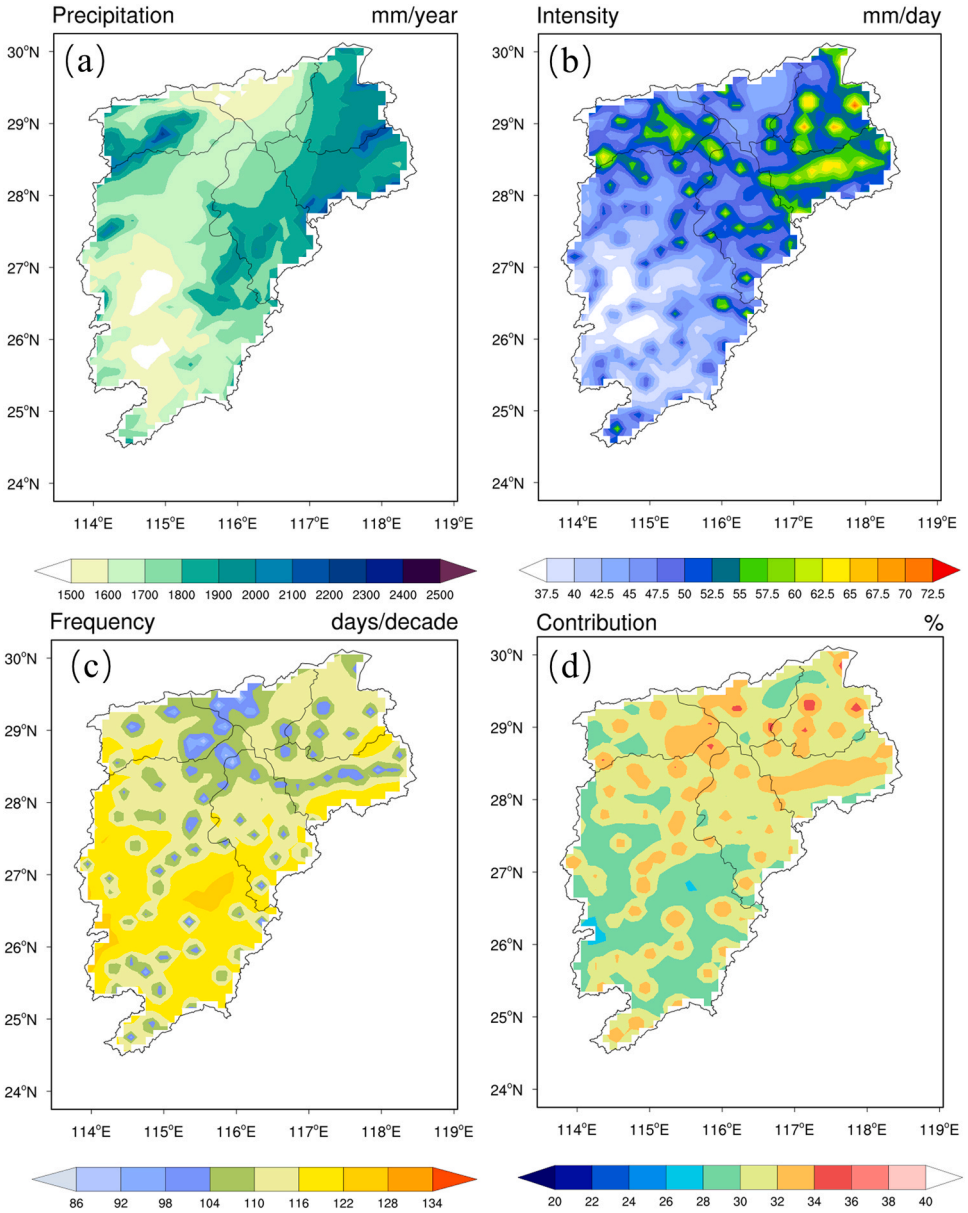

Fig. 2. Spatial distribution of (a) annual average extreme precipitation (mm/year), (b) the extreme precipitation intensity (mm/day) and (c) extreme precipitation frequency (days/decade), as well as (d) the contribution of extreme precipitation to total precipitation (%) in the period of 1983–2020.

scheme (NT scheme) is not applied to the d03 domain (3 km). The Final Operational Global Analysis (FNL) reanalysis dataset are employed as the initial and boundary fields of WRF.

2.5. Evaluation criteria

In order to effectively assess the performance of WRF simulations, precipitation observations are utilized as reference data. The evaluation metric of correlation coefficient (CC) is employed for evaluating the simulation accuracy in extreme precipitation processes (Tian et al., 2020; Zhu et al., 2023). The CC reflects the linear relationship between observed and simulated values. Higher values of CC indicate smaller errors.

3. Results

3.1. Variations of extreme precipitation intensity and frequency

Fig. 2 shows distribution characteristics of extreme precipitation in the PLB. Specifically, the high-value areas of annual average extreme precipitation were mainly located in the northeastern and northwestern parts of the basin, including the Fuhe, Raohe, Xinjiang, and Xiushui sub-basins, while the low-value areas were mainly located in the Ganjiang sub-basin (Fig. 2a). The Xinjiang and Raohe sub-basins, located in the northeastern part of the PLB, displayed the highest intensity, while the Ganjiang sub-basin exhibited the lowest intensity (Fig. 2b). The frequency of extreme precipitation in the north-central part of the PLB was lower, while it was higher

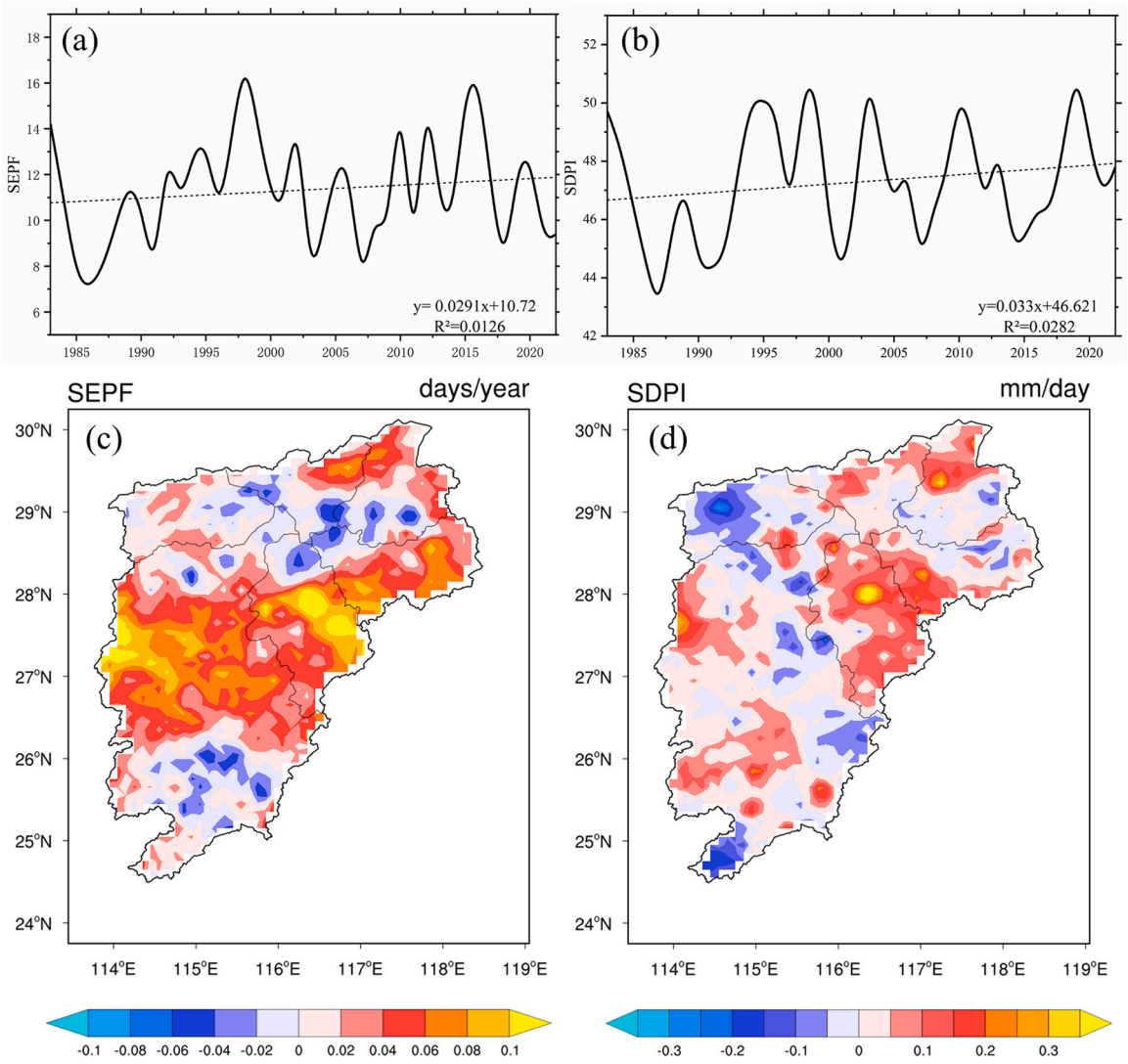

Fig. 3. (a-b) Temporal trends of the SEPF and SDPI in the period of 1983–2020. (c-d) Spatial distribution of linear trends of SEPF and SDPI.

in the southern region (Fig. 2c). Among them, extreme precipitation occurred most frequently in the Ganjiang sub-basin. This indicated that the spatial distribution of frequency and intensity showed an opposite trend.

The contribution of extreme precipitation to the total rainfall ranged from 20 % to 40 %, with the contribution rate concentrating around 30 %. Spatially, the contribution was highest in the northern part of the PLB, and lowest in most areas of the southern region, particularly in the Ganjiang sub-basin (Fig. 2d). In conclusion, the northern part of the PLB was characterized by low frequency and high intensity of extreme precipitation, as well as a high contribution to total precipitation, which resulted in the northern part being prone to more severe extreme precipitation.

The SEPF and SDPI were utilized to investigate the trend of extreme precipitation frequency and intensity in the PLB. Fig. 3a-b illustrate a general increasing trend in the frequency and intensity of extreme precipitation events from 1983 to 2022. These extreme precipitation events exhibited significant fluctuations in both SEPF and SDPI. For instance, in 1998, the frequency of extreme precipitation reached its peak at 17 days, whereas in 2007, it was as low as 7 days. The SDPI fluctuated within the range of 43–51 mm/day, with the highest value occurring in 2003 at 51 mm/day. Fig. 3c-d depict the spatial variation trends of the SEPF and SDPI indices. The SEPF index showed an increasing trend in central and northeastern parts of the PLB, primarily concentrated in the northern part of the Ganjiang sub-basin, the southern part of the Fuhe sub-basin, and the Xinjiang sub-basin. Conversely, decreasing trends were observed in the northern and southern parts of the PLB, particularly prominent in the southern part of the Ganjiang sub-basin. The SDPI index indicated little variation in extreme precipitation intensity across most areas of the PLB. However, a significant increasing trend was observed in Fuhe sub-basin for extreme precipitation intensity, while a significant weakening trend was evident in the Xiushui sub-basin.

3.2. *Spatiotemporal features of persistent and non-persistent extreme precipitation*

Fig. 4a presents the contributions of persistent and non-persistent extreme precipitation to extreme precipitation in the PLB. The PLB was generally dominated by non-persistent extreme precipitation during the period of 1983–2022. However, the contribution of persistent extreme precipitation showed a continuous increase. For instance, in 1998, the contribution of persistent extreme precipitation exceeded that of non-persistent extreme precipitation. The contributions of persistent and non-persistent extreme precipitation were similar in 2000, 2005, and 2020. The contribution rate of persistent extreme precipitation ranged from 20 % to 60 %. From 1983 to 1992, the average contribution rate was merely 30.7 %, increasing to 37.2 % from 2013 to 2022. This indicated an increasing impact of persistent extreme precipitation on the variability of extreme precipitation in the PLB. Changes in persistent and non-persistent extreme precipitation anomalies are depicted in Fig. 4b. The anomaly magnitude of persistent extreme precipitation was greater than that of non-persistent extreme precipitation. Both persistent and non-persistent extreme precipitation exhibited pronounced positive anomalies during the periods of 1990–2000 and 2010–2020. Throughout these periods, both types of extreme precipitation significantly increased, particularly in 1998 when the abnormality of PEP reached its maximum, increasing by nearly 300 mm. Additionally, non-persistent extreme precipitation exhibited its largest positive anomaly in 2010.

Fig. 5a illustrates the spatial distribution of linear trends in persistent extreme precipitation. It was found that the persistent extreme precipitation has an increasing trend in most areas of the PLB, with the most obvious increase in Fuhe sub-basin, and a decreasing trend in the northern and the southern parts of the PLB. The spatial distribution of linear trends in non-persistent extreme precipitation is presented in Fig. 5b. A significant weakening trend appeared in non-persistent extreme precipitation around Poyang Lake, along with a decrease in the southern part of the Ganjiang sub-basin. Both persistent and non-persistent extreme precipitation exhibited decreasing trends in Xiushui sub-basin, while they showed increasing trends in Fuhe sub-basin. Spatially, the contribution rate of persistent extreme precipitation to extreme precipitation demonstrated an increasing gradient from south to north (Fig. 5c). The highest contribution values observed in the northeast of the PLB, such as the Xinjiang and Raohe sub-basins, and the lowest

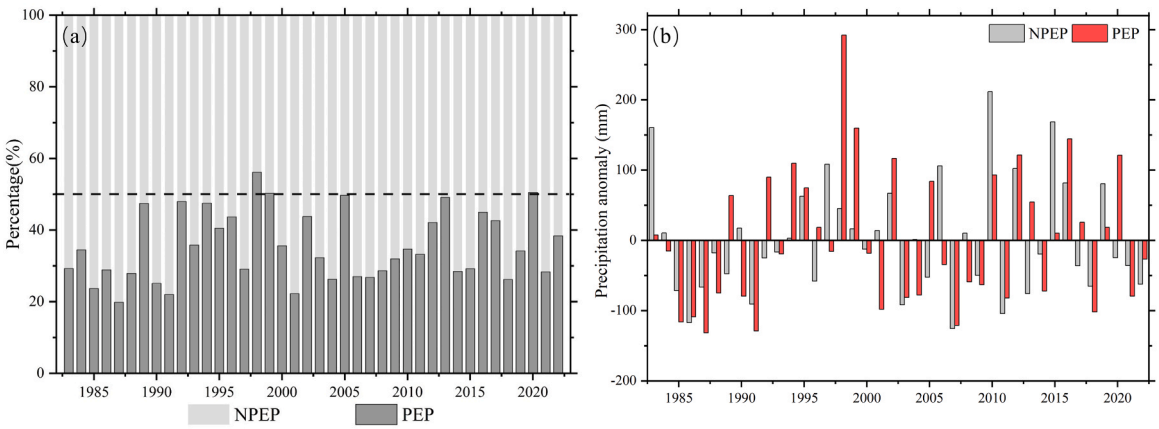

Fig. 4. (a) Contribution of persistent extreme precipitation (PEP) and non-persistent extreme precipitation (NPEP) to extreme precipitation, and (b) anomalies of PEP and NPEP in the period of 1983–2020.

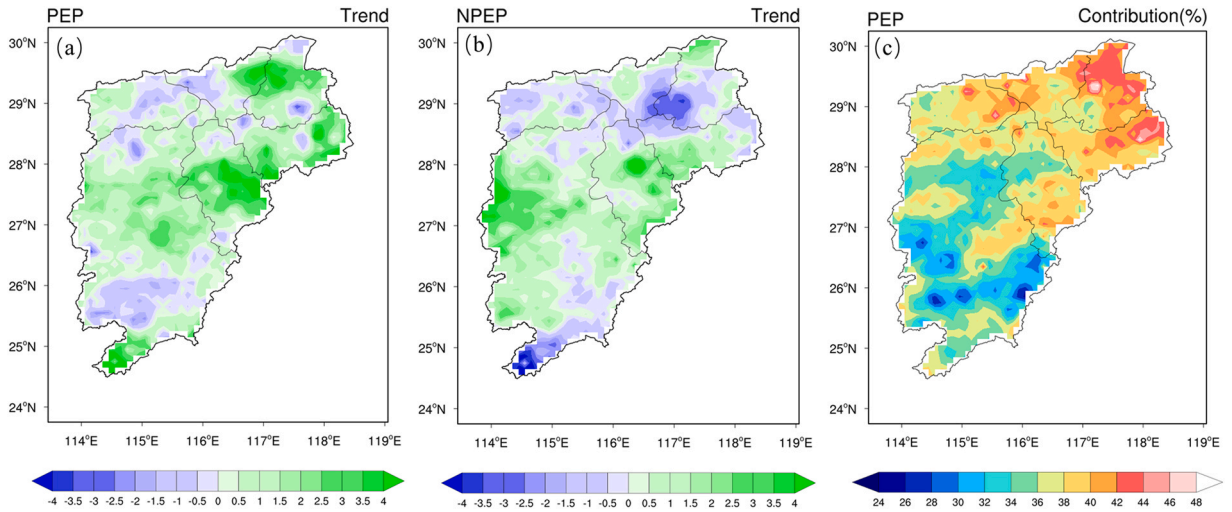

Fig. 5. Spatial distribution of trends of (a) non-persistent extreme precipitation (NPEP) and (b) persistent extreme precipitation (PEP). (c) Contribution of persistent precipitation extreme (PEP) to precipitation extreme.

contribution values observed in the southern parts of the PLB, such as the Ganjiang sub-basin. These findings showed a higher probability of persistent extreme precipitation occurrences in the northeastern sectors of the PLB. Furthermore, apart from the Ganjiang sub-basin, the contribution rates of persistent extreme precipitation in the sub-basins all exceed 30 %.

3.3. *Variations of widespread extreme precipitation events*

Fig. 6a shows the time series of the frequency for two types of widespread extreme precipitation events. Specifically, widespread extreme precipitation events that covered more than 50 percent of the grid points occurred, on average, approximately 4 days per year during the period 1983–2022, with a peak of 10 days in 2010, followed closely by 9 days in 1998. Widespread extreme precipitation events that covered more than 70 percent of the grid points had a total of 30 days within the same time period, with a maximum of 3 days observed in both 1998 and 2004. However, there was an absence of widespread extreme precipitation events during the consecutive years of 1986 and 1987. It is worth noting that both persistent and non-persistent extreme precipitation showed negative anomalies (Fig. 6b), with SDPI reaching its minimum value (Fig. 3b). These findings suggest a potential occurrence of severe droughts in the PLB during this period. Fig. 6b illustrates the monthly frequency of widespread extreme precipitation. Both types of widespread extreme precipitation were observed to be most frequent during the summer months and least frequent during winter, with a concentration in June. Widespread extreme precipitation events that covered more than 70 percent of the grid points tended to concentrate between March and June, peaking in June with up to 8 days, with no occurrences in October and November. And fewer events occurred in spring and autumn. Widespread extreme precipitation events that covered more than 50 percent of the grid points

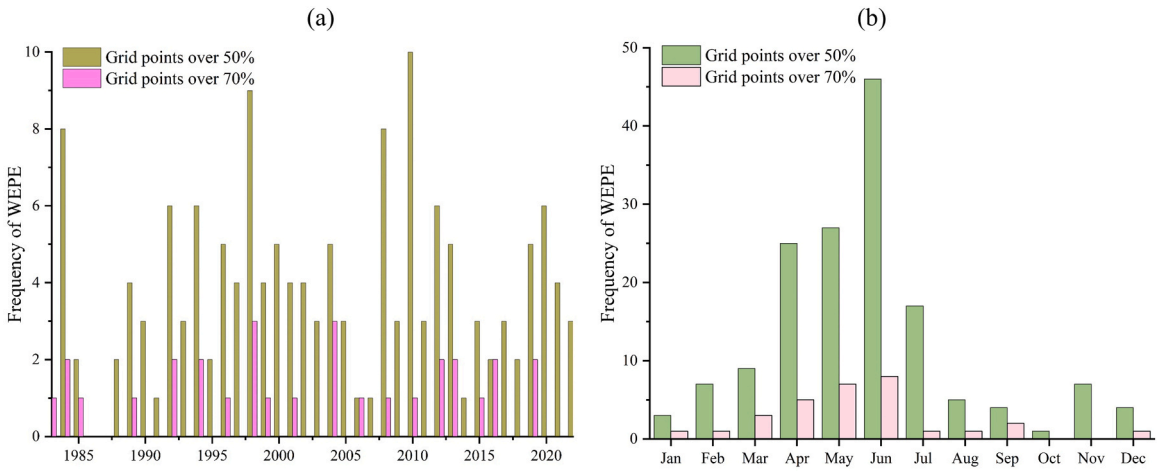

Fig. 6. (a) Annual and (b) monthly variations in the frequency of widespread extreme precipitation (WEP) event. Events with grid points exceeding 50 % and those with grid points exceeding 70 % are considered as two different types of WEP event.

were concentrated between April and July, with a maximum of 46 days in June and a minimum of one day in winter. The summer season served as the dominant period for occurrences of extreme precipitation, whereas such instances were nearly absent during the winter season.

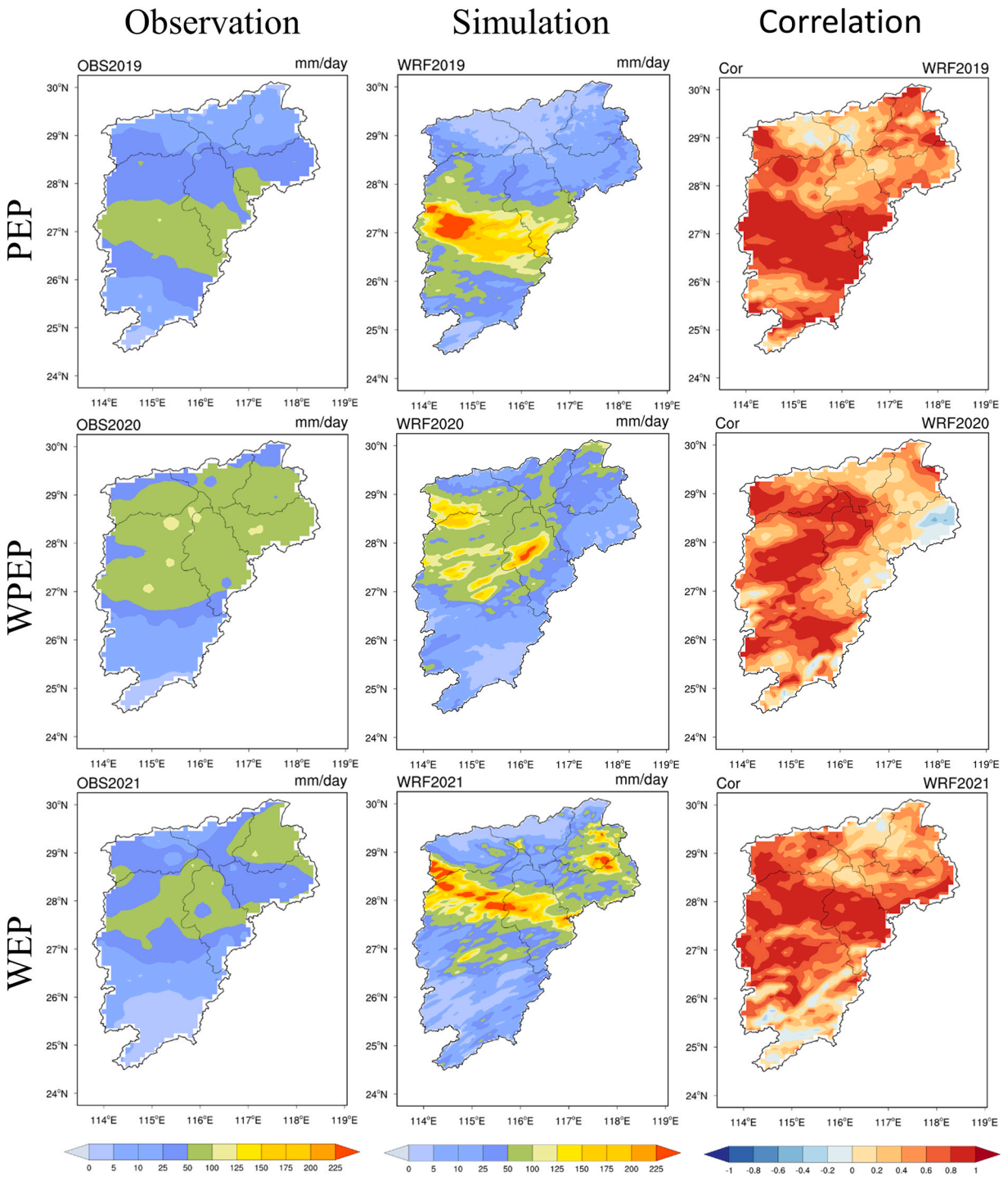

Fig. 7. Spatial distribution of observed and simulated precipitation, along with correlation coefficients for the persistent extreme precipitation in 2019, the widespread extreme precipitation in 2021, and the compound widespread-persistent extreme precipitation in 2020.

3.4. Mechanism of three different types of extreme precipitation events

Considering the possibility of simultaneous occurrence of PEP and WEP, this study identified the WPEP events during the study period of 1983–2020. The three types of extreme precipitation events were analyzed separately to identify typical events for each type. WRF was employed to investigate the surface processes and occurrence mechanisms of these extreme precipitation events. Simulation results were evaluated against observational data to verify accuracy.

Fig. 7 shows the spatial distribution of simulated and observed precipitation values and their correlation coefficients for the PEP in 2019, the WEP in 2021, and the WPEP in 2020. The spatial distributions of observed and simulated values were similar for three extreme precipitation events. During the PEP in 2019, the storm centre with high values appeared in the central part of the PLB, mainly in Ganjiang sub-basin, while the low values were primarily in the northern part of the basin. Compared to the observed values, the simulated values showed an overestimation in the western part of the Ganjiang sub-basin. For the WPEP in 2020, the storm center with high values occurred in the north-central part of the basin. The simulated values were underestimated in Xinjiang, Raohe, and Fuhe sub-basins located in the northeastern part of the PLB. For the WEP in 2021, the high-value areas were found in the central and northeastern parts of the PLB, with the simulated values overestimated in the central part of this basin. The central and northern parts of the Ganjiang sub-basin were more likely to become precipitation centers during extreme precipitation.

The correlation distributions between the simulated and observed values for different extreme precipitation (PEP, WEP, and WPEP) events exhibited similar features. The spatial patterns showed that the correlation coefficients in most areas of the PLB exceeded 0.6, especially in the central region of the basin where the correlation coefficient reached 0.8. This indicated that the simulated values were highly correlated with the observed values. However, the simulation results for the WPEP exhibited some underestimation compared to the observed values, resulting in a low correlation coefficient in the northeast of the PLB. In comparison to the WPEP, the PEP and WEP showed better performance in simulations. Overall, the simulation of extreme precipitation in most areas of the PLB showed better performance. WRF effectively captured the precipitation processes for the different extreme precipitation events. The performance of WRF in simulating extreme precipitation events over the PLB was acceptable. Therefore, the WRF simulated results can serve as a basis for exploring the different types of extreme precipitation processes.

To explore the formation mechanisms of PEP, WEP and WPEP events, this study investigated the synoptic characteristics and near-surface features during extreme precipitation events. Fig. 8 shows the temporal variations of precipitable water (PW), near-surface air temperature (T2), latent heat fluxes (LH), and water vapor mixing ratio at 2 m (Q2) associated with different extreme precipitation (PEP, WEP and WPEP) events. The trends in PW and Q2 were similar. Compared to the WPEP and WEP, the values of PW and Q2 in the PEP were the lowest. Before the occurrence of the PEP, both PW and Q2 exhibited a significant increase. When the PEP occurred, PW and Q2 reached their maximum values. After the end of extreme precipitation, both PW and Q2 rapidly decreased. However, the

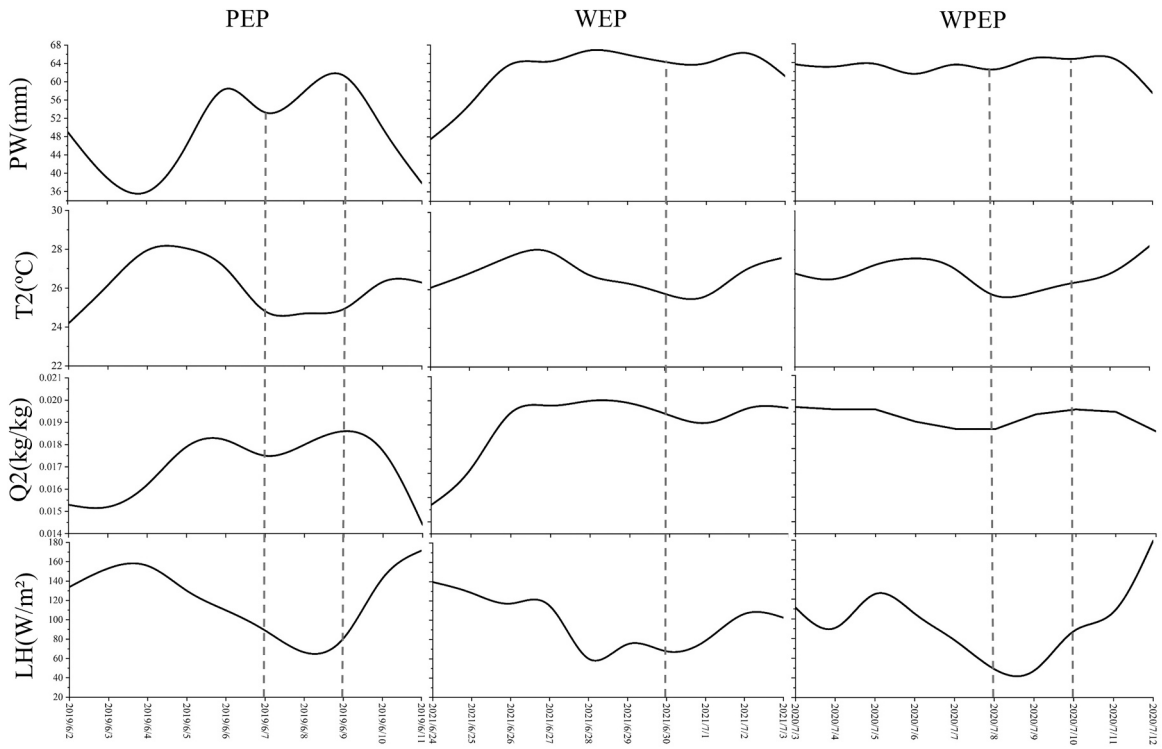

Fig. 8. Temporal variation of precipitable water (PW), temperature (T2), latent heat flux (LH), and water vapor mixing ratio at 2 m (Q2) for the PEP in 2019, the WEP in 2021, and the WPEP in 2020. The dashed lines indicate the process of extreme precipitation.

changes in PW and Q2 before and after the WEP and WPEP were relatively small. The values of the corresponding variables in the WPEP stayed at a high value for a longer period of time. Among them, Q2 ranged from 0.0185 to 0.02 kg/kg, while the PW was ranged from 61 to 66 mm. Conversely, T2 and LH exhibited a trend opposite to precipitation. The LH exhibited a trend of initially decreasing

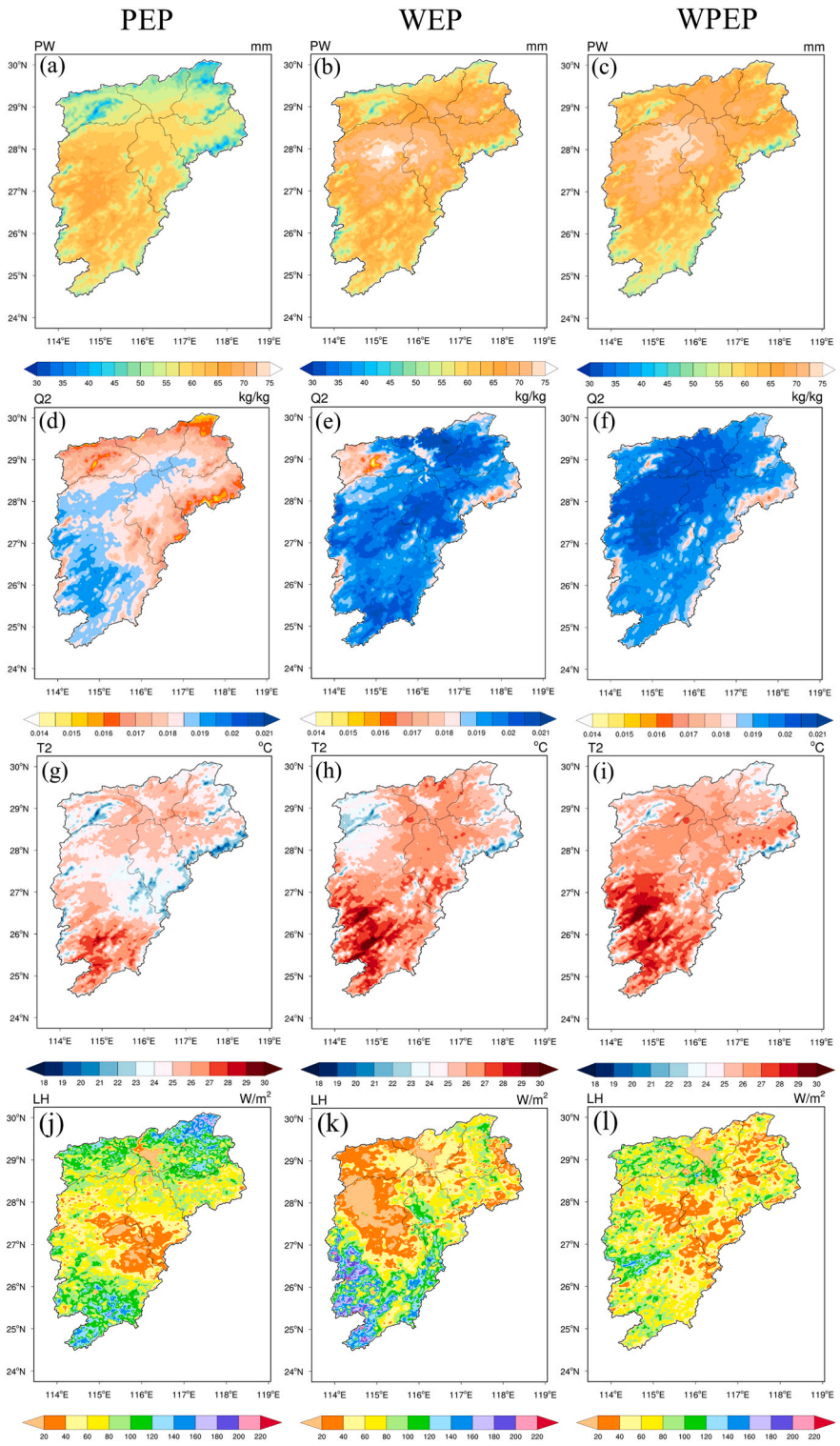

Fig. 9. Spatial distribution of (a-c) precipitable water (PW), (d-f) water vapor mixing ratio at 2 m (Q2), (g-i) temperature (T2), and (j-l) latent heat flux (LH) for the PEP in 2019, the WEP in 2021, and the WPEP in 2020.

followed by an increase, reaching its lowest value when extreme precipitation occurred. Compared to the PEP and WEP, the value of LH was the lowest in the WPEP. In general, the changes in related variables were most significant during the process of the PEP, especially for PW and Q2.

Fig. 9 shows the spatial distribution of PW, T2, LH, and Q2 during different extreme precipitation (PEP, WEP, and WPEP) events. For all extreme precipitation events, T2 was higher in the southern part of the Ganjiang sub-basin and around Poyang Lake. The low-value region of LH was found in a similar area as the high-value region of precipitation. The high-value area of PW mainly appeared in the central part of the PLB (e.g. northern part of the Ganjiang sub-basin). The spatial distributions of PW during the WEP and WPEP were similar. Compared to the WEP and WPEP events, PW in the PLB was lowest during the PEP event, particularly in the northern part of the basin, where it was below 55 mm. During the WEP, PW exceeded 60 mm in most areas of the PLB. In the WPEP, the value of Q2 in most areas of the PLB was above 0.0185 kg/kg. In particular, the value of Q2 in the northern part of the Ganjiang sub-basin and around Poyang Lake exceeded 0.02 kg/kg, which was higher than the values during the PEP and WEP. In the WEP, the spatial distribution of Q2 was different from that of PW, with high-value areas being more scattered. The spatial distribution of high-value precipitation areas in the PEP was closely aligned with the high-value regions of PW and Q2, which was mainly located in the northern part of the Ganjiang sub-basin. The high-value regions of precipitation in WPEP largely coincided with the distribution of high-value areas of PW and Q2. These differences in near-surface features may be a key factor contributing to different types of extreme precipitation events.

Adequate water vapor is considered as a critical factor in triggering extreme precipitation events. Here, water vapor within the atmospheric layer spanning from 300 hPa to 1000 hPa was opted to compute the vertical integral water vapor flux and divergence based on the distribution characteristics of water vapor. Fig. 10 shows changes in water vapor transport during the PEP, WEP, and WPEP events. In three different types of extreme precipitation events, water vapor was mainly originated from the southwest, with strong moisture transport, which led to convergence over the PLB. Prior to the WEP and WPEP events, two streams of water vapor from the north and southwest converged in the northern part of the basin, leading to higher water vapor accumulation over the northern part of the PLB, which was conducive to the occurrence of extreme precipitation events. As precipitation occurred, the water vapor in the north weakened, and the location of water vapor convergence gradually moved from the northwest to the northeast of the PLB. After the extreme precipitation terminated, only southwest water vapor appeared over the basin. However, during the PEP, the water vapor over the PLB mainly flowed from the southwest direction.

Furthermore, the precursor signals of atmospheric changes were crucial to improve understanding of triggering mechanisms for extreme precipitation occurrence. Fig. 11 shows the evolution of sea-level pressure and wind prior to the PEP, WEP and WPEP. Before the occurrence of the PEP, a sea-level depression on the surface was observed in the vicinity of the PLB, with a small low-pressure range

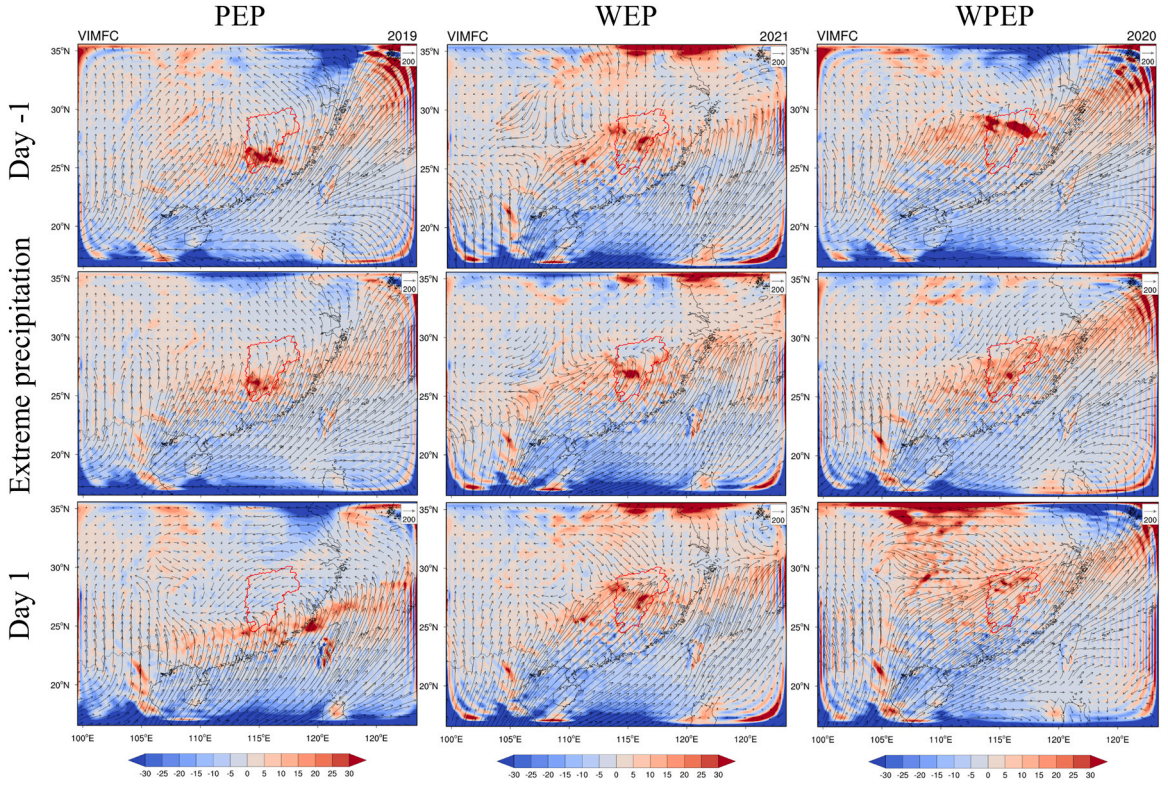

Fig. 10. Vertically integrated water vapor flux (VIWVF, vectors, units: kg. m^{-1}. s^{-1}) and water vapor flux divergence (units: 10^{-5} kg. m^{-2}. s^{-1}) during the PEP in 2019, the WEP in 2021, and the WPEP in 2020.

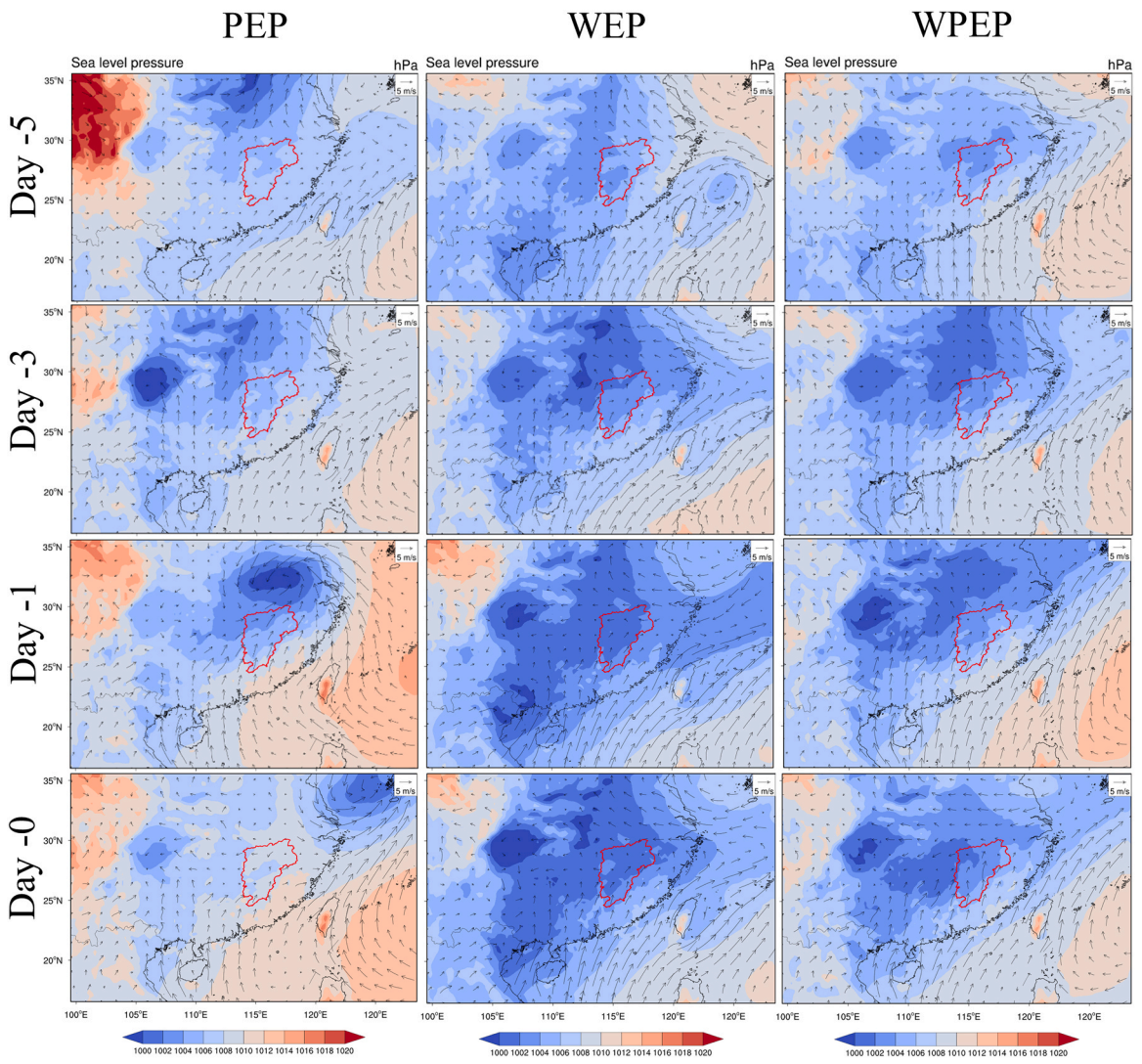

Fig. 11. Evolution of sea-level pressure and wind before the PEP in 2019, the WEP in 2021, and the WPEP in 2020. Day −0 denotes the occurrence of extreme precipitation, Day −1 denotes 1 day before the day when extreme precipitation begins, and so forth. The red outline indicates the boundary of the PLB.

(day −3). The sea-level depression gradually moved from the northwest to the northeast. When precipitation began, the sea-level depression gradually moved away from the PLB. Prior to the WPEP and WEP, a low-pressure center developed to the northwest of the PLB. Over time, this low-pressure system intensified and expanded near the basin, causing a greater influence on the PLB. The emergence of sea-level depression was an important surface feature before the occurrence of extreme precipitation events.

Fig. 12 shows the variations of 500 hPa geopotential height before the PEP, WEP and WPEP. The 500 hPa geopotential height field indicated a region of lower geopotential heights to the north. The variation of the low-value area of 500hPa geopotential height affected the transport of water vapor. Prior to the occurrence of extreme precipitation, a region of low geopotential height values was observed in the northeast of the PLB at the 500 hPa level. Influenced by this low-pressure system in the northeast, water vapor flowed over the PLB from the southwest, indicating the significant influence of large-scale circulation on the formation and evolution of extreme precipitation in this basin. In general, the water vapor from the southwest provided sufficient water vapor conditions over the PLB for three extreme precipitation events. The occurrence of extreme precipitation was closely associated with the surface low-pressure systems, as well as the variations in the low-value area of the 500 hPa geopotential height.

4. Discussion

Although the frequency of extreme precipitation events occurring in the PLB shows no significant change, the intensity of precipitation has increased, suggesting an increasing probability of intense extreme precipitation events occurring within the PLB. Further

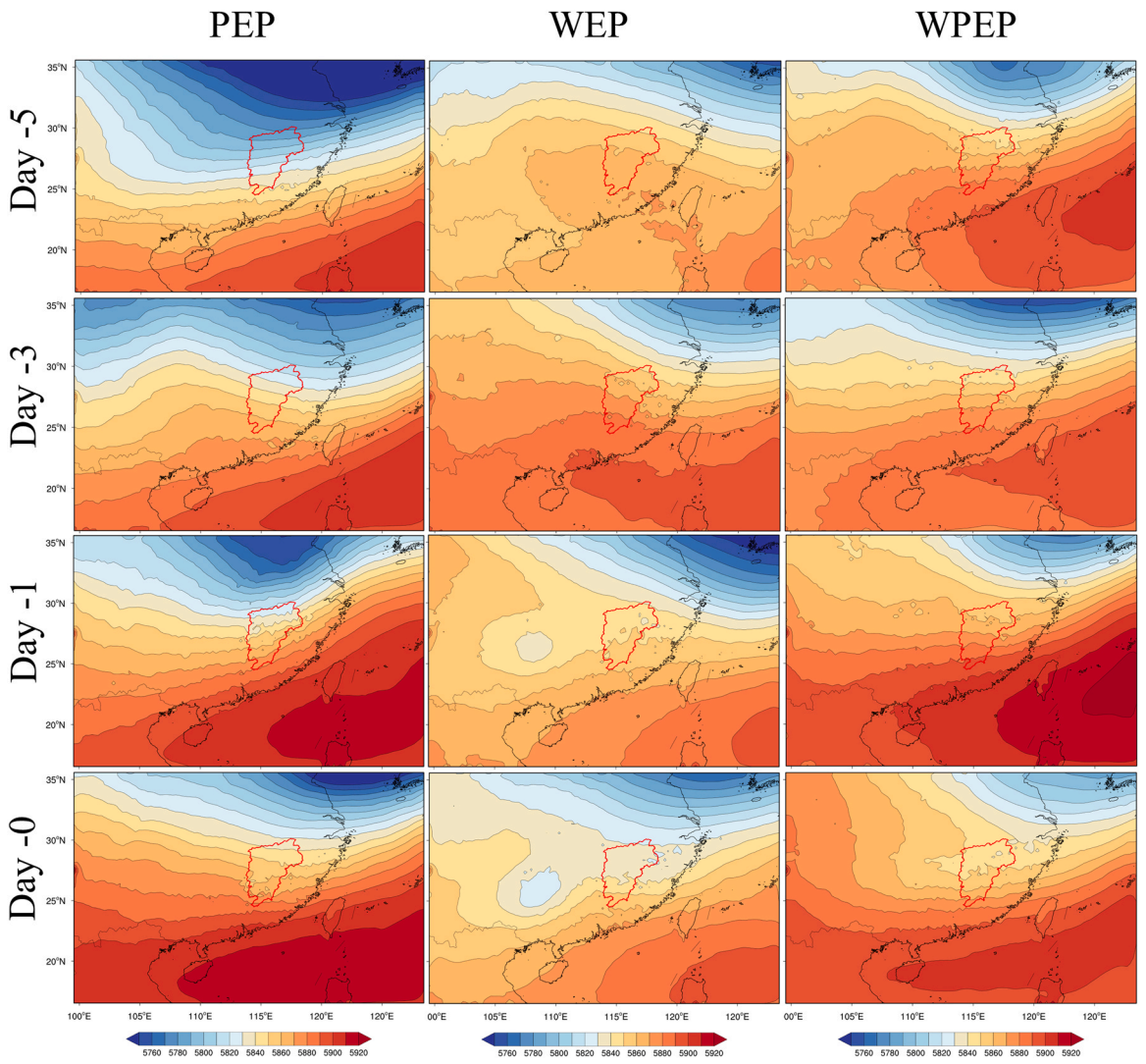

Fig. 12. As Fig. 11 but for 500 hPa geopotential height. The red outline is the boundary of the PLB.

investigation revealed that although the basin was generally dominated by non-persistent extreme precipitation, the proportion of persistent extreme precipitation was continuously increasing within the PLB. This discovery is similar to the findings that the frequency and intensity of regional persistent extreme precipitation in China have been increasing, with the affected areas primarily concentrated in the Yangtze River, Huai River, and South China regions (Wan et al., 2017; He and Zhai, 2018; Du et al., 2019). In certain years, there are considerable fluctuations in the number of widespread extreme precipitation events within the PLB. The sub-basins of Xiushui, Raohe, and Xinjiang in the northern part of the PLB are identified as hotspots, which are highly susceptible to extreme rainfall-related disasters in the future. The increased susceptibility to extreme precipitation in the northern part of the PLB may be attributed to the influence of large-scale circulation patterns (Ding et al., 2020; Li et al., 2021; Wu et al., 2023). Previous studies has found that climate indices such as ENSO, NAO, IOD, and PDO have a significant impact on extreme precipitation in the PLB(Zhang et al., 2014; Zhang et al., 2016; Liu et al., 2017). The movement direction and duration of rain belts under the influence of subtropical high-pressure systems are also driving factors in contributing to widespread or localized extreme precipitation. However, it is not excluded that extreme precipitation is complicated by regional factors (Lei et al., 2021). Although under the same large-scale circulation factors, there are differences in the occurrence mechanisms of different types of extreme precipitation.

In our study, significant differences in surface characteristics were observed prior to the occurrence of the three different types of extreme precipitation. Before the occurrence of the PEP, a rapid increase in PW and Q2 is observed. However, during WPEP, both PW and Q2 remain at their highest values, suggesting that higher atmospheric water vapor content may contribute to more severe extreme precipitation. The high-value areas of extreme precipitation are influenced by the spatial distribution of Q2 and PW. The variations in PW and Q2 are considered as important precursors to the occurrence of extreme precipitation (Bao et al., 2017; Kunkel et al., 2020; Su and Smith, 2021). The precipitation in the PLB is primarily influenced by water vapor transported from the southwest in summer,

driven by abundant moisture from the Indian Ocean. The specific variations in water vapor during extreme precipitation events are often overlooked. In the PEP event, water vapor originates solely from the southwest. However, in the WEP and WPEP, two branches of water vapor converge from the north and southwest, indicating that such convergence is more likely to result in large-scale precipitation. This highlights the critical role of synoptic conditions and water sources in triggering extreme precipitation. (Waliser and Guan, 2017; Tan et al., 2019; Vázquez et al., 2020). Compared to ordinary extreme precipitation events, the PEP, WEP, and WPEP events result in more serious disasters, particularly more serious flood events. Exploring the connection between different types of extreme precipitation and their associated flood impacts would be an interesting topic for further research. Despite the case study of typical extreme precipitation events utilized in this paper contributes to the understanding of the characteristics and triggering mechanisms of extreme precipitation in the PLB. It is necessary for subsequent studies to explore the impacts of PEP, WEP, and WPEP in a more comprehensive way.

Similar to the previous simulated results, WRF is able to capture the different types of extreme precipitation in this study (Yang et al., 2021; Gao et al., 2022; Deng et al., 2023). However, WRF simulations exhibit varying performance in PEP, WEP, and WPEP events. Among the different events, the largest error is observed in the WPEP event, primarily due to the underestimation of simulated values in the northeastern region of the PLB. Compared to single-type extreme precipitation events, the WRF model has greater difficulty accurately capturing compound extreme precipitation events. Therefore, it is necessary to improve the parameter settings of the WRF model in future study to enhance the simulation accuracy of compound widespread-persistent extreme precipitation.

5. Conclusions

This study investigated the changes in intensity and frequency of extreme precipitation and compared the occurrence of temporal extreme precipitation, spatial extreme precipitation and compound temporal-spatial extreme precipitation events in the PLB of China. The physical mechanisms of extreme precipitation were explored through WRF simulations of the PEP, WEP and WPEP events. The findings would contribute to our understanding of regional land-atmosphere interactions in the occurrence and development of extreme precipitation events. The main conclusions are summarized as follows.

(1) The intensity of extreme precipitation exhibited a distribution pattern of high in the northern region and low in the southern region of the PLB. Extreme precipitation events characterized by higher intensity and severity were more likely to occur in the northern part of the PLB. The contribution of extreme precipitation to total rainfall ranged from 20 % to 40 %, with a higher contribution of extreme precipitation in the north than in the south. Overall, the frequency and intensity of extreme precipitation within the PLB showed an increasing trend over time, with significant fluctuations. The SEPF showed an increasing trend in the central and northeastern part of the PLB, and a decrease in the southern and northwestern part of the PLB. The SDPI significantly increased in Fuhe sub-basin and decreased in Xiushui sub-basin.

(2) The contribution of persistent extreme precipitation increased from an average of 30.7 % in the period 1983–1992–37.2 % in the period 2013–2022. The impact of persistent extreme precipitation on total extreme precipitation was growing. The contribution of persistent extreme precipitation tended to increase spatially from south to north, with the largest contribution in the Xinjiang and Raohe sub-basins located in the northeastern part of the PLB. The PLB was still dominated by non-persistent extreme precipitation. In addition, the magnitude of persistent extreme precipitation anomalies was larger than those of non-persistent extreme precipitation anomalies.

(3) The average frequency of widespread extreme precipitation events (covering more than 50 % of grid points) was 4 days per year, with the most frequent occurrence of 10 days in 2010. The widespread extreme precipitation events (covering more than 70 % of grid points) appeared on a total of 30 days during the study period, with the highest number of events occurring in 1998 and 2004. The widespread extreme precipitation events occurred most frequently in the summer and least in the winter, with a concentration in the month of June.

(4) The high-value precipitation area during the PEP was found in the central part of the Ganjiang sub-basin, whereas during WEP and WPEP, the area of high-value precipitation was observed in the north-central part of the PLB. The features of PW and Q2 increased continuously prior to the PEP. However, the changes in PW and Q2 for the WEP and WPEP events were relatively small. The low-value region of LH exhibited similar distribution characteristics with the high-value region of PW. During the PEP event, the PLB was influenced only by water vapor from the southwest. In contrast, during WEP and WPEP events, two water vapor streams from the north and southwest impacted the PLB, with expanded sea level low pressure coverage preceding the events. The variation in the low value of 500 hPa geopotential height was closely related to the occurrence of extreme precipitation.

CRediT authorship contribution statement

Kunstmann Harald: Supervision, Conceptualization. **Gao Lu:** Writing – review & editing, Supervision, Project administration, Funding acquisition, Conceptualization. **Chen Ying:** Writing – review & editing, Investigation. **Wei Jianhui:** Validation, Data curation. **Zhang Yinchi:** Software, Methodology, Data curation. **Ma Miaomiao:** Methodology, Investigation, Data curation. **Deng Chao:** Writing – original draft, Software, Methodology, Investigation, Conceptualization.

Declaration of Competing Interest

The authors declare that they have no known competing financial interests or personal relationships that could have appeared to influence the work reported in this paper.

Acknowledgments

This work was supported by the National Natural Science Foundation of China (Grant No. 42271030), Fujian Provincial Funds for Distinguished Young Scientists (Grant No. 2022J06018) and "Young Eagle Plan" Top Talents of Fujian Province. The operation of WRF model was supported by the High Performance Computing Center of Fujian Normal University. The precipitation data were provided by National Tibetan Plateau/ Third Pole Environment Data Center (http://data.tpdc.ac.cn).

Data availability

Data will be made available on request.

References

Bao, J.W., Sherwood, S.C., Alexander, L.V., Evans, J.P., 2017. Future increases in extreme precipitation exceed observed scaling rates. Nat. Clim. Change 7, 128. https://doi.org/10.1038/nclimate3201.

Cassano, J.J., Cassano, E.N., Seefeldt, M.W., Gutowski Jr., W.J., Glisan, J.M., 2016. Synoptic conditions during wintertime temperature extremes in Alaska. J. Geophys. Res. Atmospheres 121, 3241–3262. https://doi.org/10.1002/2015jd024404.

Cheng, Q.P., Jin, H.Y., Ren, Y.T., 2023. Persistent and nonpersistent regional extreme total, daytime, and night-time precipitation events over southwest China (1961-2019). Int. J. Climatol. 43, 2150–2174. https://doi.org/10.1002/joc.7968.

Deng, C., Chi, Y.X., Huang, Y.S., Jiang, C.Y., Su, L.J., Lin, H., Jiang, L.Z., Guan, X.J., Gao, L., 2023. Sensitivity of WRF multiple parameterization schemes to extreme precipitation event over the Poyang Lake Basin of China. Front. Environ. Sci. 10, 1102864. https://doi.org/10.3389/fenvs.2022.1102864.

Deng, C., Lin, T.S., Zhuang, Y., Zhang, Y.C., Guan, X.J., Jiang, L.Z., Chen, Y., Gao, L., 2024. Onset of flash drought based on the WRF in the Poyang Lake Basin of China. Atmos. Res. 309, 107547. https://doi.org/10.1016/j.atmosres.2024.107547.

Ding, Y.H., Liang, P., Liu, Y.J., Zhang, Y.C., 2020. Multiscale variability of Meiyu and Its Prediction: a new review. J. Geophys. Res. Atmospheres 125, e2019JD031496. https://doi.org/10.1029/2019jd031496.

Donat, M.G., Lowry, A.L., Alexander, L.V., O'Gorman, P.A., Maher, N., 2016. More extreme precipitation in the world's dry and wet regions. Nat. Clim. Change 6, 508. https://doi.org/10.1038/nclimate2941.

Dong, Q., Chen, X., Chen, T.X., 2011. Characteristics and changes of extreme precipitation in the Yellow-Huaihe and Yangtze-Huaihe Rivers Basins, China. J. Clim. 24, 3781–3795. https://doi.org/10.1175/2010jcli3653.1.

Du, H., Alexander, L.V., Donat, M.G., Lippmann, T., Srivastava, A., Salinger, J., Kruger, A., Choi, G., He, H.S., Fujibe, F., Rusticucci, M., Nandintsetseg, B., Manzanas, R., Rehman, S., Abbas, F., Zhai, P., Yabi, I., Stambaugh, M.C., Wang, S., Batbold, A., de Oliveira, P.T., Adrees, M., Hou, W., Zong, S., Santos, e Silva, Lucio, C.M., Wu, Z, P.S., 2019. Precipitation from persistent extremes is increasing in most regions and globally. Geophys. Res. Lett. 46, 6041–6049. https://doi.org/10.1029/2019gl081898.

Gao, L., Wei, J., Lei, X., Ma, M., Wang, L., Guan, X., Lin, H., 2022. Simulation of an extreme precipitation event using ensemble-based WRF model in the southeastern coastal Region of China. Atmosphere 13. https://doi.org/10.3390/atmos13020194.

Glisan, J.M., Gutowski Jr., W.J., Cassano, J.J., Higgins, M.E., 2013. Effects of spectral nudging in WRF on arctic temperature and precipitation simulations. J. Clim. 26, 3985–3999. https://doi.org/10.1175/jcli-d-12-00318.1.

Gou, J.J., Miao, C.Y., Samaniego, L., Xiao, M., Wu, J.W., Guo, X.Y., 2021. CNRD v1.0: a high-quality natural runoff dataset for hydrological and climate studies in China. Bull. Am. Meteorol. Soc. 102, E929–E947. https://doi.org/10.1175/bams-d-20-0094.1.

Gründemann, G.J., Zorzetto, E., Beck, H.E., Schleiss, M., van de Giesen, N., Marani, M., van der Ent, R.J., 2023. Extreme precipitation return levels for multiple durations on a global scale. J. Hydrol. 621, 129558. https://doi.org/10.1016/j.jhydrol.2023.129558.

Han, J., Miao, C., Gou, J., Zheng, H., Zhang, Q., Guo, X., 2023. A new daily gridded precipitation dataset for the Chinese mainland based on gauge observations. Earth Syst. Sci. Data 15, 3147–3161. https://doi.org/10.5194/essd-15-3147-2023.

He, B.-R., Zhai, P.-M., 2018. Changes in persistent and non-persistent extreme precipitation in China from 1961 to 2016. Adv. Clim. Change Res. 9, 177–184. https://doi.org/10.1016/j.accre.2018.08.002.

Janssen, E., Sriver, R.L., Wuebbles, D.J., Kunkel, K.E., 2016. Seasonal and regional variations in extreme precipitation event frequency using CMIP5. Geophys. Res. Lett. 43, 5385–5393. https://doi.org/10.1002/2016gl069151.

Jiang, Q., Li, W.Y., Fan, Z.D., He, X.G., Sun, W.W., Chen, S., Wen, J.H., Gao, J., Wang, J., 2021. Evaluation of the ERA5 reanalysis precipitation dataset over Chinese Mainland. J. Hydrol. 595, 125660. https://doi.org/10.1016/j.jhydrol.2020.125660.

Kang, H., Sridhar, V., Ali, S.A., 2022. Climate change impacts on conventional and flash droughts in the Mekong River Basin. Sci. Total Environ. 838, 155845. https://doi.org/10.1016/j.scitotenv.2022.155845.

Kunkel, K.E., Stevens, S.E., Stevens, L.E., Karl, T.R., 2020. Observed climatological relationships of extreme daily precipitation events with precipitable water and vertical velocity in the contiguous United States. Geophys. Res. Lett. 47, e2019GL086721. https://doi.org/10.1029/2019gl086721.

Lei, X.Y., Gao, L., Ma, M.M., Wei, J.H., Xu, L.G., Wang, L., Lin, H., 2021. Does non-stationarity of extreme precipitation exist in the Poyang Lake Basin of China? J. Hydrol. Reg. Stud. 37, 100920. https://doi.org/10.1016/j.ejrh.2021.100920.

Lesk, C., Rowhani, P., Ramankutty, N., 2016. Influence of extreme weather disasters on global crop production. Nature 529, 84. https://doi.org/10.1038/nature16467.

Li, X., Hu, Q., 2019. Spatiotemporal changes in extreme precipitation and its dependence on topography over the Poyang Lake Basin, China. Adv. Meteorol. 2019, 1253932. https://doi.org/10.1155/2019/1253932.

Li, X., Zhang, K., Gu, P.R., Feng, H.T., Yin, Y.F., Chen, W., Cheng, B.C., 2021. Changes in precipitation extremes in the Yangtze River Basin during 1960-2019 and the association with global warming, ENSO, and local effects. Sci. Total Environ. 760, 144244. https://doi.org/10.1016/j.scitotenv.2020.144244.

Liu, J.Y., Zhang, Q., Singh, V.P., Gu, X.H., Shi, P.J., 2017. Nonstationarity and clustering of flood characteristics and relations with the climate indices in the Poyang Lake basin, China. Hydrol. Sci. J. 62, 1809–1824. https://doi.org/10.1080/02626667.2017.1349909.

Miao, C.Y., Gou, J.J., Fu, B.J., Tang, Q.H., Duan, Q.Y., Chen, Z.S., Lei, H.M., Chen, J., Guo, J.L., Borthwick, A.G.L., Ding, W.F., Duan, X.W., Li, Y.G., Kong, D.X., Guo, X. Y., Wu, J.W., 2022. High-quality reconstruction of China's natural streamflow. Sci. Bull. 67, 547–556. https://doi.org/10.1016/j.scib.2021.09.022.

Moore, B.J., Keyser, D., Bosart, L.F., 2019. Linkages between extreme precipitation events in the central and Eastern United States and Rossby Wave Breaking. Mon. Weather Rev. 147, 3327–3349. https://doi.org/10.1175/mwr-d-19-0047.1.

Myhre, G., Alterskjaer, K., Stjern, C.W., Hodnebrog, O., Marelle, L., Samset, B.H., Sillmann, J., Schaller, N., Fischer, E., Schulz, M., Stohl, A., 2019. Frequency of extreme precipitation increases extensively with event rareness under global warming. Sci. Rep. 9, 16063. https://doi.org/10.1038/s41598-019-52277-4.

Ning, G., Luo, M., Zhang, Q., Wang, S., Liu, Z., Yang, Y., Wu, S., Zeng, Z., 2021. Understanding the mechanisms of summer extreme precipitation events in Xinjiang of Arid Northwest China. J. Geophys. Res. Atmospheres 126, e2020JD034111. https://doi.org/10.1029/2020jd034111.

Ojeda, M.G.V., Gamiz-Fortis, S.R., Castro-Diez, Y., Esteban-Parra, M.J., 2017. Evaluation of WRF capability to detect dry and wet periods in Spain using drought indices. J. Geophys. Res. Atmospheres 122, 1569–1594. https://doi.org/10.1002/2016jd025683.

Ombadi, M., Risser, M.D., Rhoades, A.M., Varadharajan, C., 2023. A warming-induced reduction in snow fraction amplifies rainfall extremes. Nature. https://doi.org/10.1038/s41586-023-06092-7.

Pal, L., Ojha, C.S.P., Dimri, A.P., 2021. Characterizing rainfall occurrence in India: natural variability and recent trends. J. Hydrol. 603, 126979. https://doi.org/10.1016/j.jhydrol.2021.126979.
Papalexiou, S.M., Montanari, A., 2019. Global and regional increase of precipitation extremes under global warming. Water Resour. Res. 55, 4901–4914. https://doi.org/10.1029/2018wr024067.
Pei, F., Wu, C., Liu, X., Hu, Z., Xia, Y., Liu, L.-A., Wang, K., Zhou, Y., Xu, L., 2018. Detection and attribution of extreme precipitation changes from 1961 to 2012 in the Yangtze River Delta in China. Catena 169, 183–194. https://doi.org/10.1016/j.catena.2018.05.038.
Rastogi, D., Touma, D., Evans, K.J., Ashfaq, M., 2020. Shift toward intense and widespread precipitation events over the United States by Mid-21st Century. Geophys. Res. Lett. 47, e2020GL089899. https://doi.org/10.1029/2020gl089899.
Roxy, M.K., Ghosh, S., Pathak, A., Athulya, R., Mujumdar, M., Murtugudde, R., Terray, P., Rajeevan, M., 2017. A threefold rise in widespread extreme rain events over central India. Nat. Commun. 8, 708. https://doi.org/10.1038/s41467-017-00744-9.
Shibuya, R., Takayabu, Y., Kamahori, H., 2021. Dynamics of widespread extreme precipitation events and the associated large-scale environment using AMeDAS and JRA-55 Data. J. Clim. 34, 8955–8970. https://doi.org/10.1175/jcli-d-21-0064.1.
Smalley, K.M., Glisan, J.M., Gutowski, W.J., 2019. Alaska daily extreme precipitation processes in a subset of CMIP5 global climate models. J. Geophys. Res. Atmospheres 124, 4584–4600. https://doi.org/10.1029/2018jd028643.
Su, Y.B., Smith, J.A., 2021. An atmospheric water balance perspective on extreme rainfall potential for the contiguous US. Water Resour. Res. 57, e2020WR028387. https://doi.org/10.1029/2020wr028387.
Sun, J.Q., Ao, J., 2013. Changes in precipitation and extreme precipitation in a warming environment in China. Chin. Sci. Bull. 58, 1395–1401. https://doi.org/10.1007/s11434-012-5542-z.
Tan, X.Z., Gan, T.Y., Chen, S., Horton, D.E., Chen, X.H., Liu, B.J., Lin, K.R., 2019. Trends in persistent seasonal-scale atmospheric circulation patterns responsible for seasonal precipitation totals and occurrences of precipitation extremes over Canada. J. Clim. 32, 7105–7126. https://doi.org/10.1175/jcli-d-18-0408.1.
Tan, X.Z., Wu, X.X., Huang, Z.Q., Fu, J.Y., Tan, X.J., Deng, S.M., Liu, Y.X., Gan, T.Y., Liu, B.J., 2023. Increasing global precipitation whiplash due to anthropogenic greenhouse gas emissions. Nat. Commun. 14, 2796. https://doi.org/10.1038/s41467-023-38510-9.
Tang, G.Q., Zeng, Z.Y., Ma, M.H., Liu, R.H., Wen, Y.X., Hong, Y., 2017. Can near-real-time satellite precipitation products capture rainstorms and guide flood warning for the 2016 Summer in South China? IEEE Geosci. Remote Sens. Lett. 14, 1208–1212. https://doi.org/10.1109/lgrs.2017.2702137.
Thackeray, C.W., Hall, A., Norris, J., Chen, D., 2022. Constraining the increased frequency of global precipitation extremes under warming. Nat. Clim. Change 12, 441. https://doi.org/10.1038/s41558-022-01329-1.
Tian, L., Jin, J., Wu, P., Niu, G.-y, Zhao, C., 2020. High-resolution simulations of mean and extreme precipitation with WRF for the soil-erosive Loess Plateau. Clim. Dyn. 54, 3489–3506. https://doi.org/10.1007/s00382-020-05178-6.
Tuel, A., Steinfeld, D., Ali, S.M., Sprenger, M., Martius, O., 2022. Large-scale drivers of persistent extreme weather during early summer 2021 in Europe. Geophys. Res. Lett. 49, e2022GL099624. https://doi.org/10.1029/2022gl099624.
Vázquez, M., Nieto, R., Liberato, M.L.R., Gimeno, L., 2020. Atmospheric moisture sources associated with extreme precipitation during the peak precipitation month. Weather Clim. Extrem. 30, 100289. https://doi.org/10.1016/j.wace.2020.100289.
Waliser, D., Guan, B., 2017. Extreme winds and precipitation during landfall of atmospheric rivers. Nat. Geosci. 10, 179–U183. https://doi.org/10.1038/ngeo2894.
Wan, B., Gao, Z., Chen, F., Lu, C., 2017. Impact of Tibetan Plateau surface heating on persistent extreme precipitation events in southeastern China. Mon. Weather Rev. 145, 3485–3505. https://doi.org/10.1175/mwr-d-17-0061.1.
Wu, Q., Zheng, Z.H., Li, L., Wu, S.S., Liu, Y.A., 2023. Prediction skill and predictability of precipitation during Meiyu and rainy season in North China using ECMWF subseasonal forecasts. Clim. Dyn. https://doi.org/10.1007/s00382-023-06863-y.
Xie, T.J., Ding, T., Wang, J., Zhang, Y.J., Gao, H., Zhao, X.L., Zhao, L., 2023. Weather pattern conducive to the extreme summer heat in North China and driven by atmospheric teleconnections. Environ. Res. Lett. 18, 104025. https://doi.org/10.1088/1748-9326/acfaaf.
Yang, H., Liu, M., Wang, M., Qin, P., Fang, S., 2022. Projections of extreme precipitation in the middle and upper Yangtze River at 1.5 °C and 2 °C warming thresholds based on bias correction. Theor. Appl. Climatol. 147, 1589–1600. https://doi.org/10.1007/s00704-021-03899-0.
Yang, Q.Y., Yu, Z.B., Wei, J.H., Yang, C.G., Gu, H.H., Xiao, M.Z., Shang, S.S., Dong, N.P., Gao, L., Arnault, J., Laux, P., Kunstmann, H., 2021. Performance of the WRF model in simulating intense precipitation events over the Hanjiang River Basin, China - A multi-physics ensemble approach. Atmos. Res. 248, 105206. https://doi.org/10.1016/j.atmosres.2020.105206.
Yin, J.B., Gentine, P., Zhou, S., Sullivan, S.C., Wang, R., Zhang, Y., Guo, S.L., 2018. Large increase in global storm runoff extremes driven by climate and anthropogenic changes. Nat. Commun. 9, 4389. https://doi.org/10.1038/s41467-018-06765-2.
Zhang, Z.X., Chen, X., Xu, C.Y., Hong, Y., Hardy, J., Sun, Z.H., 2015. Examining the influence of river-lake interaction on the drought and water resources in the Poyang Lake basin. J. Hydrol. 522, 510–521. https://doi.org/10.1016/j.jhydrol.2015.01.008.
Zhang, Q., Gu, X.H., Singh, V.P., Shi, P.J., Luo, M., 2017. Timing of floods in southeastern China: seasonal properties and potential causes. J. Hydrol. 552, 732–744. https://doi.org/10.1016/j.jhydrol.2017.07.039.
Zhang, Q., Xiao, M.Z., Singh, V.P., Chen, Y.D., 2014. Max-stable based evaluation of impacts of climate indices on extreme precipitation processes across the Poyang Lake basin, China. Glob. Planet. Change 122, 271–281. https://doi.org/10.1016/j.gloplacha.2014.09.005.
Zhang, Q., Xiao, M.Z., Singh, V.P., Wang, Y.Q., 2016. Spatiotemporal variations of temperature and precipitation extremes in the Poyang Lake basin, China. Theor. Appl. Climatol. 124, 855–864. https://doi.org/10.1007/s00704-015-1470-6.
Zhong, Y., Tian, B., Kim, H., Yuan, X., Liu, X., Zhu, E., Wu, Y., Wang, L., Wang, L., 2025. Over 60% precipitation transformed into terrestrial water storage in global river basins from 2002 to 2021. Commun. Earth Environ. 6 (1), 53. https://doi.org/10.1038/s43247-024-01967-7.
Zhu, K., Yu, B., Xue, M., Zhou, B., Hu, X.-M., 2021. Summer season precipitation biases in 4 km WRF forecasts over southern China: diagnoses of the causes of biases. J. Geophys. Res. Atmospheres 126, e2021JD035530. https://doi.org/10.1029/2021jd035530.
Zhu, T., Zhang, W., Wang, J., Chen, Y., Xin, S., Zhu, J., 2023. Investigating spatial variations of compound heat-precipitation events in guangdong, china through a convection-permitting model. Remote Sens. 15, 4745. https://doi.org/10.3390/rs15194745.